Surface Recombination Noise in InAs/GaSb Superlattice Photodiodes

2013 Appl. Phys. Express 6 032202

(http://iopscience.iop.org/1882-0786/6/3/032202)

Applied Physics Express 6 (2013) 032202
http://dx.doi.org/10.7567/APEX.6.032202

Surface Recombination Noise in InAs/GaSb Superlattice Photodiodes

Tunay Tansel[1]*, Kutlu Kutluer[1], Abdullah Muti[2], Ömer Salihoglu[2], Atila Aydinli[2], and Rasit Turan[1]

[1]*Department of Physics, Middle East Technical University (METU), 06531 Ankara, Turkey*
[2]*Department of Physics, Advanced Research Laboratories, Bilkent University, 06800 Ankara, Turkey*
E-mail: tutansel@metu.edu.tr

Received January 11, 2013; accepted February 14, 2013; published online March 7, 2013

The standard Schottky noise approach alone is not sufficient to describe the noise mechanism in an InAs/GaSb superlattice photodetector at reverse negative bias. The additional noise identified appears at surface activation energies below 60 meV and is inversely proportional to the reverse bias. In order to satisfactorily explain the experimental data, we hereby propose the existence of a surface recombination noise that is a function of both the frequency and bias. The calculated noise characteristics indeed show good agreement with the experimental data.

Mid-wavelength-infrared (MWIR) InAs/GaSb superlattice (SL) photodetectors are attracting considerable attention due to their promise for new generation infrared detectors with applications in industrial and medical technologies. This is due to the fact that these photodetectors offer remarkable advantages over other types of MWIR detectors, including low noise current thanks to the suppression of Auger recombination.[1)]

However, in spite of numerous studies on SL detectors with different features,[2)] the effects of surface leakage current on the detector performance are not fully understood. In general, the existence of surface states at the crystal surface due to abrupt termination of the semiconductor surface leads to leakage current that can limit the SL infrared detector performance. This is of great importance, especially where the detector area approaches the dimensions needed for focal-plane-array applications. Consequently, intentional passivation is needed for mesa-etched detectors to suppress the leakage current by minimizing the surface states and, hence, the influence of foreign materials.[3,4)] The relation between surface leakage and noise properties of the SL detector needs to be clarified for a complete understanding of its noise behavior and to optimize the passivation. The noise figure performance is one of the most sensitively affected parameters by both the bulk and surface regions of detectors.[5,6)] This means that better understanding of the noise properties of a SL will lead to the significant reduction of noise, e.g., $1/f$ noise.

Here, we reveal the surface effects in MWIR InAs/GaSb SL photodetectors by studying the device performance through the relationship between the spectral noise level and the surface passivation, and describe the surface limited current mechanism under reverse bias conditions.

InAs/GaSb SL detector structures designed for MWIR operation (with cut-off wavelength 4.9 μm at 79 K) were grown by IQE Inc. The device structures were grown by molecular beam epitaxy on an n-type (001) GaSb substrate, based on 60 periods n-type/60 periods of a non-intentionally doped (n.i.d.) active region/90 periods of a p-type InAs/GaSb SL. Each period in the entire structure consists of 2.85 nm InAs and 3.30 nm GaSb layers with InSb-like interfaces. GaSb layers in the p-type superlattice period were doped with Be to a level of $1.5 \times 10^{17}\,\mathrm{cm}^{-3}$ while the InAs layers were doped with Te to a level of $5 \times 10^{17}\,\mathrm{cm}^{-3}$. The entire SL structure was enclosed by a 20 nm n-type InAs: Te ($5 \times 10^{17}\,\mathrm{cm}^{-3}$) top and a 1 μm thick p-type GaSb: Be ($1 \times 10^{17}\,\mathrm{cm}^{-3}$) bottom contact layers.[7)]

$400 \times 400\,\mu\mathrm{m}^2$ mesa structures were wet etched using a phosphoric acid based solution. Surface passivation was realized directly after wet etching by growing either 230 nm SiO_2 or 150 nm Si_3Ni_4 as a passivation layer via the plasma enhanced chemical vapor deposition (PECVD) at the sample temperature of 423 K. A Ti–Au (5 nm/200 nm) bilayer was then evaporated to both the top and the bottom of the photodiodes to achieve ohmic contacts. The contact resistances were 3 and 7 Ω for the n- and p-type contacts, respectively. Details of the complete fabrication processes can be found elsewhere.[8,9)]

In order to measure the temperature-dependent dark current or the resistance-area (RA) product, a CTI Cryogenics helium cryostat (Cryodyne Refrigeration System 22C) was employed as a cold head and a Keithley (Keithley 6487) picoammeter was used to apply the DC bias (V_{bias}) to the detector and to read the output current.

For the dark current noise characterizations, specimens were placed in a cryostat and cooled to 79 K using liquid nitrogen. During the measurements all the instruments including the low noise current amplifier (Stanford Research Systems SR570), cryostat, and fast fourier transform (FFT) spectrum analyzer (Stanford Research Systems SR760) were placed inside a shielded and grounded box. The dark noise current as a function of bias was measured at a frequency of ~40 Hz. We subtracted the system noise from the measured total noise (I_{total}) to obtain the detector noise. Here, the detector noise sources consist of the *white noise* as well as an *additional low frequency noise* related to the frequency range above the white noise level.[10)] Schottky noise ($I^2_{\mathrm{SN}} = 2qI$) and Johnson noise ($I^2_{\mathrm{JN}} = 4k_{\mathrm{B}}T/R_{\mathrm{d}}$) together form the "white noise" ($I^2_{\mathrm{SN}} + I^2_{\mathrm{JN}}$) of the detector, where q is the electronic charge constant, I the dark current, k_{B} the Boltzmann constant, T the temperature, and R_{d} the dark differential resistance.

The low-temperature (79 K) dark current–voltage (I–V) characteristics of the SL detectors with different passivation layers and an unpassivated surface are shown in Fig. 1. At −0.5 V bias voltage, the unpassivated, and passivated samples. The dark current increases proportionally with the reverse bias for unpassivated and Si_3N_4-passivated devices. The best results were obtained from the SiO_2 passivated devices whose dark current decreased by up to 1 to 3 orders of magnitude in comparison.

In order to understand the above offset in the I–V characteristics between different passivation layers (see Fig. 1), we studied the dark noise characteristics of these devices

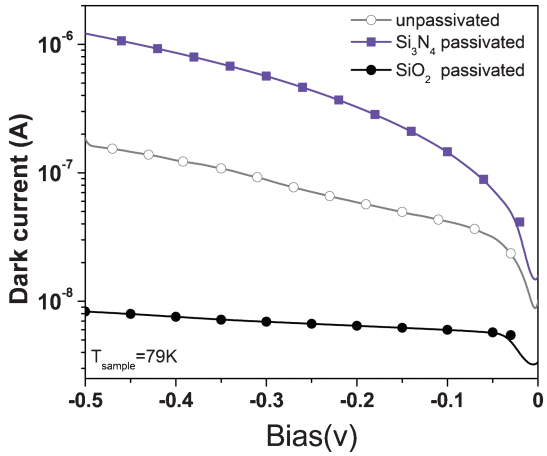

Fig. 1. Dark current vs V_{Bias} for SL devices at 79 K.

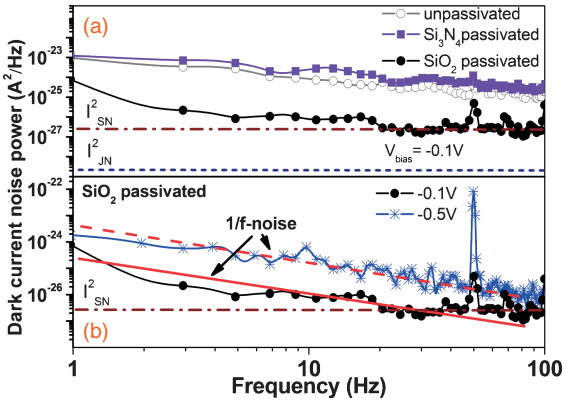

Fig. 2. Noise spectra as function of frequency for SL detectors at 79 K (a) at −0.1 V. The peaks at 50–100 Hz are due to electronic noise and its harmonics. (b) at −0.1 and −0.5 V (temperature 79 K). The fitted straight line and dotted lines indicate the $1/f$-noise behavior.

over the 1 to 100 Hz frequency range. Figure 2(a) shows the noise spectra at 79 K for the unpassivated, Si_3N_4- and SiO_2-passivated SL detectors at 0.1 V bias. For the SiO_2-passivated device, the frequency independent plateau in the 20–100 Hz range is due to the *white noise*. This is well matched with the calculated theoretical Schottky noise ($I^2_{SN} = 2.5 \times 10^{-27}$ A^2/Hz). The dark current noise of low-frequency noise (*additional noise* current) increases as the frequency decreases ($1/f$ noise) below 40 Hz. It is important to note that $1/f$ noise does not intrinsically present itself in InAs/GaSb SL photodiode structures,[11] and therefore, $1/f$ noise is affected by the surface. Moreover, it is particularly sensitive to surface leakage currents emanating from surface states as described above.[3,6] The *additional noise* current is suppressed while the dark noise current is reduced by an order of magnitude (at −0.1 V bias) in the SiO_2 passivated device with respect to unpassivated and Si_3N_4-passivated detectors [see Fig. 2(a)]. The effects of surface states along the exposed mesa surface seem to be reduced by the SiO_2-passivation. In contrast, the noise value for the Si_3N_4-passivated sample exhibits a frequency-dependent behavior that confirms the contribution of *additional low-frequency noise*. Thus, it appears that Si_3N_4-passivation degrades the sample surface quality.[12]

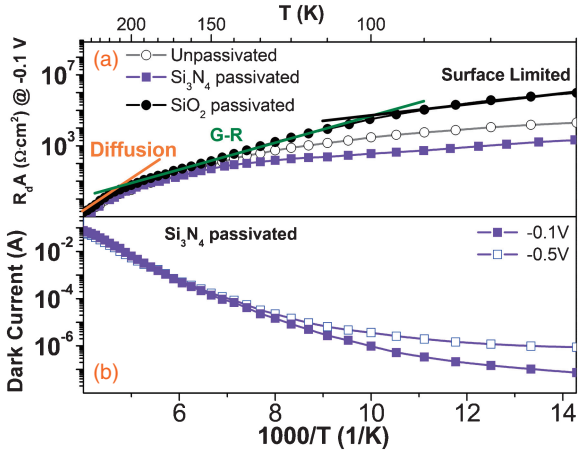

Fig. 3. (a) Inverse temperature vs resistance-area product for unpassivated, and passivated SL photodetectors, displaying three distinct regimes with different dominant current mechanisms: bulk diffusion from 150 to 200 K, generation–recombination from 95 to 150 K, and surface-limited sector below 95 K. (b) Dark Current vs inverse temperature curves obtained for Si_3N_4-passivated SL detectors at −0.1 and −0.5 V bias voltages.

Figure 2(b) shows the increment of the dark and *additional low-frequency noise* currents at different reverse bias voltages for the SiO_2-passivated SL devices. At 40 Hz, the dark noise current value of the −0.5 V curve is approximately 3 times higher than that of the −0.1 V curve. An *additional low frequency noise* section begins to dominate the spectra after −0.2 V bias and increases with the reverse bias at 79 K. This means that the increment of the *low-frequency noise* part of the spectrum is influenced by the applying reverse bias voltage. Therefore, we may say that applied reverse bias can also influence surface leakage current of the device since the additional *low-frequency noise* is sensitive/proportional to the surface leakage current as mentioned above.

In order to investigate the effect of the surface leakage current at 79 K, we performed dark I–V measurements on a series of diodes with varying perimeter-to-area ratios, since the surface resistivity is inversely proportional to the surface-dependent leakage current in photodiodes.[12] The measured surface resistivities at zero bias were 8×10^5, 2×10^4, and 1×10^6 Ω·cm for unpassivated, Si_3N_4-passivated, and SiO_2-passivated devices, respectively. These results clearly show that SiO_2-passivation can suppress the surface leakage current by about an order of magnitude, by satisfying surface states and consequently preventing surface currents. In contrast, Si_3N_4-passivation does not improve the surface resistivity significantly. The obtained surface resistivity values explain the differences observed with the dark current measurements (see Fig. 1) for unpassivated and passivated samples (at zero bias).

Alternatively, in order to clarify the dominant current mechanism in the temperature range of interest, the RA vs reciprocal temperature ($1000/T$) plot is obtained [Fig. 3(a)], which can separate the bulk current from the surface current components.[13] It can be inferred that since the samples vary only in terms of the passivation material, any deviation of the curves from the bulk diffusion and the GR trend indicates the onset of surface leakage due to the fact that

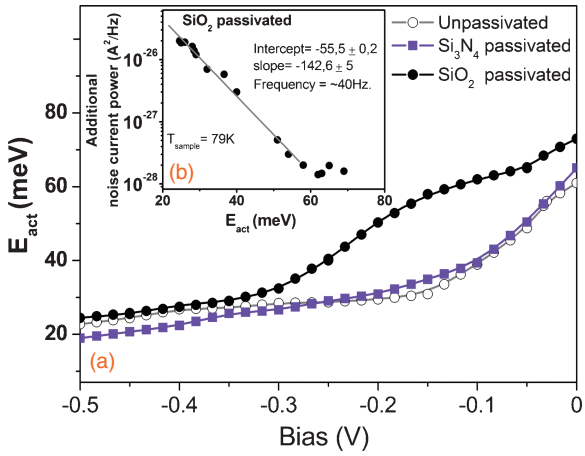

Fig. 4. (a) Activation energy vs applied reverse bias for unpassivated and passivated devices. The activation energy decreases with applied reverse bias. (b) Additional noise current power vs activation energy passivated sample at reverse biases from 0 to 0.5 V. The additional noise current increases linearly in a log scale with decreasing E_{act} between −0.18 and −0.5 V. Curve fitting is used to determine the value of I_c wich is the intercept (where E_{act} is zero) divided by $2q$ and whereby the slope can be denoted as $1/k_BT$.

deviation from the Arrhenius fit is related to the presence of surface-limited current.[11,14)]

The activation energy (E_{act}) is calculated from the slope of the linear fit to $\ln(RA)$ vs $1000/T$ graph.[15,16)] The bulk diffusion E_a is 0.24 eV, which is very close to the cut-off wavelength obtained from optical measurements for all samples. The GR E_{act} is 0.12 eV (for SiO_2-passivated sample), which is half of the band gap as expected in the literature.[16)] For different passivations, different deviations from the Arrhenius fit were observed for the temperature range of 65–95 K. In this temperature range and at −0.1 V bias, the surface-limited current is 1–2 orders of magnitude suppressed in the SiO_2-passivated device while Si_3N_4 passivation increases it by about an order of magnitude in comparison with the unpassivated device. Hence, the deviations seen in Fig. 3(a) are an indicator of the surface leakage current and will be further discussed below [Fig. 3(b)] as a function of reverse bias voltage.

Figure 3(b) shows the deviation more clearly in the Arrhenius fit for Si_3N_4 passivation at various reverse biases in the temperature range of 65–95 K. In accordance with Ref. 13, the higher the reverse bias, the more the surface states become active since the surface leakage current is a direct result of surface states. Therefore, by considering the results obtained from Figs. 2(b) and 3(b) in combination, we can relate the surface states to the additional *low-frequency noise*.

In order to better understand the influence of bias voltage on surface states, next we investigate this influence in terms of E_{act} on reverse bias voltage, V_{bias}, [see Fig. 4(a)]. It shows that at zero bias, the E_{act} is 61, 65, and 72 meV for unpassivated, Si_3N_4-passivated and SiO_2-passivated devices, respectively. It should be noted that for all three curves, the maximum E_{act} is above 60 meV at zero bias. At −0.1 V, E_{act} for surface-limited current is around 60 meV for SiO_2, which is half of the generation–recombination (GR) E_{act}, meanwhile, E_{act} of Si_3N_4-passivated and unpassivated devices for surface-limited currents is ∼40 meV, which is one-third that of lower than SiO_2 passivated samples. A further increase of V_{bias} to −0.5 V lowers E_{act} to around 20 meV for all devices. Clearly, an inverse dependence is seen between E_{act} and V_{bias} for all samples. This effect can be viewed to result in the additional noise seen in Figs. 2(a) and 2(b) for all devices. It is pronounced for the surface activation energy of <60 meV. Therefore, we can conclude that this lowering of E_{act} by reverse bias leads to the appearance of the *additional noise*, assuming that a decrease in E_{act} involves an increase in the number of charge carriers flowing to the surface and recombining. This effect can be attributed to a surface recombination noise (I_{SRN}), in agreement with Ref. 17.

By claiming that all the noise sources are statistically independent, where the total noise I_{total} is then found as: $I^2_{total} = I^2_{SN} + I^2_{JN} + I^2_{SRN}$, square sum of all noise sources.

Figure 4(b) shows the dependence of additional dark noise current as well as recombination noise ($I^2_{SRN} = I^2_{total} - I^2_{SN} - I^2_{JN}$) on E_{act}. It reveals that the additional noise current increases exponentially as E_{act} decreases. We note that decreasing surface E_{act} with V_{bias} causes higher surface recombination noise, which acts as an independent noise source. This additional $1/f$ noise [see Figs. 2(a) and 2(b)] is dominant at E_{act} of <60 meV. Due to the fact that this is a consequence of a recombination process, no additional current flow can be seen in I–V characteristics. This noise is thus only apparent in direct noise measurements.

It is reasonable to suggest that surface recombination noise could be related to the surface carrier concentration (n_s), which should be dependent on the operating V_{bias} for a given temperature. Moreover, we expect an exponential dependence of E_{act} [see Fig. 4(b)] on n_s as $n_s \sim \exp(-E_{act}/k_BT)$.[16,18)] From this assumption, the leakage current, I_{lc} (A), can be written as $I_{lc} = I_c \exp(-E_{act}/k_BT)$, where I_c is a prefactor.

According to Ref. 19, the surface recombination noise I_{SRN} of SL photodiodes can be calculated by using

$$I^2_{SRN} = 2qI_{lc} = I_c \exp(-E_{act}/k_BT), \quad (1)$$

I_c is a frequency-dependent proportionality prefactor and it can be deduced from Fig. 4(b). More precisely, I_c is the total number of surface charge carriers (which may lead to a recombination) per unit time, and $\exp(-E_{act}/k_BT)$ is the probability that any given surface carrier will result in a recombination in the surface states. The temporal fluctuation in the recombination rate per unit time itself leads to frequency dependence behavior which in turn results in surface recombination noise I_{SRN}. We propose roughly inverse frequency dependence variation such as $\sinh(\Delta f/f)$ where Δf is the decay frequency constant, but it is not clear exactly how the frequency dependence of I_c varies; therefore, further investigations are needed.

To demonstrate the validity of Eq. (1), it is fitted to the experimental dark current noise in the voltage range of 0 to −0.5 V, as shown in Fig. 5. It illustrates the comparison between Schottky noise and measured dark noise current as a function of the bias for both unpassivated and passivated SL devices at around 40 Hz. It can be seen that for all curves at zero bias (in the Johnson-noise-limited range), there are

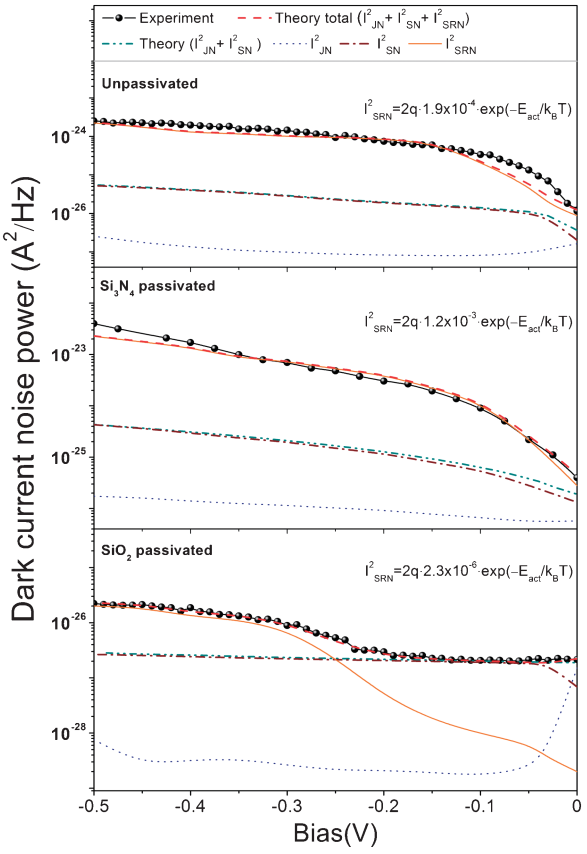

Fig. 5. Dark noise currents power as function of the reverse bias at 79 K for the both unpassivated, passivated devices. The dashed-dotted line denotes the (I^2_{JN}); the dotted-line represents the (I^2_{JN}) noise: the dash-dot-dot-line demonstrates the theoretical calculated *white noise* theory; solid-line demonstrates the theoretical calculated surface recombination noise (I^2_{SRN}) noise and the *white noise* together (Theory total, dashed-line). The calculated noise fits well with the measured noise (Experiment).

no significant deviations from the theoretically expected noise current values. As mentioned before in relation to Fig. 2(a), the *additional* noise does not exist at −0.1 V bias for 40 Hz frequency [see also Fig. 4(b)], where the dominant noise is the Schottky-noise for the SiO_2-passivated device. However, at higher biases (in the Schottky-noise-dominated range), in all the devices, the measured dark noise current values deviate from the theoretically expected values. These deviations for unpassivated, Si_3N_4-passivated and SiO_2-passivated devices are respectively 7, 10, and 3 times higher than the expected Schottky noise values at −0.5 V. This is because of the drastic increase of the *low-frequency noise* ($1/f$ noise) at the higher reverse bias, which was clearly seen for SiO_2 passivation in Fig. 2(b).

In order to explain the characteristics plot in noise calculations (see Fig. 5), we deduced all the necessary parameters, such as E_{act}, I_c, I_{SN}, and I_{JN}, from the experimental data. This resulted in a good agreement between the fitted and experimental curves for all SL diodes studied. This agreement strongly suggests that the *additional* dark current noise originates from the carrier recombination at the surface for given E_{act}, T, and V_{bias}.

In conclusion, we showed that SiO_2 passivation suppresses the dark current by up to two orders of magnitude, which could be attributed to the effective passivation of surface states. Contrary to the commonly expected noise behavior, a difference was observed between the experimental and calculated Schottky-noise for reverse voltages. The *additional* $1/f$ noise is attributed to the presence of surface leakage current, which emanated from the decrease in the activation energy at the device surface with the applied reverse V_{bias}. In order to provide agreement between theoretical and experimental noise values, we proposed that surface recombination noise is a function of both voltage and frequency.

1) A. Rogalski: Prog. Quantum Electron. **27** (2003) 59.
2) O. Salihoglu, A. Muti, K. Kutluer, T. Tansel, R. Turan, Y. Ergun, and A. Aydinli: Appl. Phys. Lett. **101** (2012) 073505.
3) O. Salihoglu, A. Muti, K. Kutluer, T. Tansel, R. Turan, and A. Aydinli: J. Phys. D **45** (2012) 365102.
4) R. Chaghi, C. Cervera, H. Ait-Kaci, P. Grech, J. B. Rodriguez, and P. Christol: Semicond. Sci. Technol. **24** (2009) 065010.
5) B. K. Jones: Adv. Electron. Electron Phys. **87** (1993) 201.
6) M. B. Weissman: Rev. Mod. Phys. **60** (1988) 537.
7) T. Tansel, K. Kutluer, O. Salihoglu, A. Aydinli, B. Aslan, B. Arikan, M. C. Kilinc, Y. Ergun, U. Serincan, and R. Turan: IEEE Photonics Technol. Lett. **24** (2012) 790.
8) A. Gin, Y. Wei, J. Bae, A. Hood, J. Nah, and M. Razeghi: Thin Solid Films **447–448** (2004) 489.
9) O. Salihoglu, A. Muti, K. Kutluer, T. Tansel, R. Turan, C. Kocabas, and A. Aydinli: J. Appl. Phys. **111** (2012) 074509.
10) K. Jaworowicz, I. Ribet-Mohammed, C. Cervera, J. B. Rodriguez, and P. Christol: IEEE Photonics Technol. Lett. **23** (2011) 242.
11) A. Soibel, D. Z.-Y. Ting, C. J. Hill, M. Lee, J. Nguyen, S. A. Keo, J. M. Mumolo, and S. D. Gunapala: Appl. Phys. Lett. **96** (2010) 111102.
12) E. Plis, M. N. Kutty, S. Myers, H. S. Kim, N. Gautam, L. R. Dawson, and S. Krishna: Infrared Phys. Technol. **54** (2011) 252.
13) B. M. Nguyen, D. Hoffman, E. K.-W. Huang, S. Bogdanov, P. Y. Delaunay, M. Razeghi, and M. Z. Tidrow: Appl. Phys. Lett. **94** (2009) 223506.
14) E. K. Huang, D. Hoffman, B. Nguyen, P. Delaunay, and M. Razeghi: Appl. Phys. Lett. **94** (2009) 053506.
15) G. Marre, B. Vinter, and V. Berger: Semicond. Sci. Technol. **18** (2003) 284.
16) S. Mou, J. V. Li, and S. L. Chung: J. Appl. Phys. **102** (2007) 066103.
17) A. Van Der Ziel: Proc. IEEE **58** (1970) 1178.
18) M. Weinelt, M. Kutschera, R. Schmidt, C. Orth, T. Fauster, and M. Rohlfing: Appl. Phys. A **80** (2005) 995.
19) C. A. Vergers: *Handbook of Electrical Noise: Measurement and Technology* (TAB Books, 1987) 2nd ed.